VI-G Photoionization and Photodissociation Dynamics Studied by Electron and Fluorescence Spectroscopy

Molecular photoionization is a major phenomenon in vacuum UV excitation and provides a large amount of information on fundamental electron-core interactions in molecules. Especially, neutral resonance states become of main interest, since they often dominate photoabsorption cross sections and lead to various vibronic states which are inaccessible in direct ionization. We have developed a versatile machine for two-dimensional photoelectron spectroscopy in order to elucidate dynamical aspects of superexcited states such as autoionization, resonance Auger decay, predissociation, vibronic couplings, and internal conversion. In a two-dimensional photoelectron spectrum (2D-PES), the photoelectron yield is measured as a function of both photon energy $E_{h\nu}$ and electron kinetic energy E_k (binding energy). The spectrum, usually represented as a contour plot, contains rich information on photoionization dynamics.

Photofragmentation into ionic and/or neutral species is also one of the most important phenomena in the vacuum UV excitation. In some cases, the fragments possess sufficient internal energy to de-excite radiatively by emitting UV or visible fluorescence. It is widely accepted that fluorescence spectroscopy is an important tool to determine the fragments and to clarify the mechanisms governing the dissociation processes of diatomic and polyatomic molecules. For several years we have concentrated our energies on fluorescence spectroscopy of H_2O in the photon energy region of 15–55 eV.

VI-G-1 Photofragmentaion Mechanisms of H_2O Studied by Ultraviolet Dispersed Spectroscopy

MITSUKE, Koichiro

[*J. Electron Spectrosc. Relat. Phenom.* **144-147**, 131–133 (2005)]

Fragmentation of H_2O has been studied by dispersed fluorescence spectroscopy at excitation photon energies above 20 eV.[1)] In dispersed spectra several vibrational bands begin to emerge below 320 nm with an appearance energy of $h\nu \sim 30$ eV. We have assigned these peaks to OH($A^2\Sigma^+ \rightarrow X\ ^2\Pi$) transition, judging from characteristic peaks due to the R_1 band heads for the $\Delta v = v' - v'' = 0$ sequence at 306.4, 312.6, and 318.8 nm. The counter fragment of OH($A^2\Sigma^+$) must be H*(n) in the Rydberg state ($n \geq 2$). The above appearance energy is much higher than the dissociation limits for the OH ($A^2\Sigma^+$) + H*($n \geq 2$) channels, but in good agreement with the vertical transition energies[2)] for the associated Rydberg states of H_2O. There exist salient hydrogen atomic lines at $h\nu \geq 24.5$ eV constituting the Balmer series with n = 3–9, as indicated in Figure 1. The dispersed spectra reveal that there is no appreciable fluorescence signal from OH($A^2\Sigma^+$) below 30 eV. Hence, the dissociation channel of OH($A^2\Sigma^+$) + H*(n) is not responsible for the Balmer emission at $h\nu$ = 24.5–30 eV. The most plausible process leading to this Balmer emission is the three-body dissociation to H*($n \geq 3$) + H(n = 1) + O(^3P_g), which has the thermochemical threshold at 21.7 eV with n = 3.

References

1) K. Mitsuke, *J. Chem. Phys.* **117**, 8334–8340 (2002).
2) J. Appell and J. Durup, *Int. J. Mass Spectrom. Ion Phys.* **10**, 247–265 (1972/73).

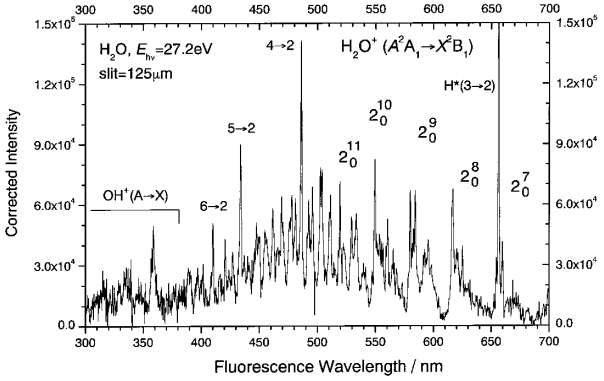

Figure 1. Dispersed fluorescence spectra of H_2O measured at $h\nu$ = 27.2 eV. The $2_0^{\nu_2'}$ symbols designate the vibrational progression in the bending mode ν_2 of the $H_2O^+[\tilde{A}\ ^2A_1 (0,\nu_2',0) \rightarrow \tilde{X}\ ^2B_1\ (0,0,0)]$ transition. The hydrogen Balmer lines H*[$n\ ^2L'_{J'} \rightarrow 2^2L''_{J''}$ (n = 3–9)]are indicated by the ($n \rightarrow$ 2) marks.

VI-H Extreme UV Photoionization Studies of Fullerenes by Using a Grazing-Incidence Monochromator and High-Temperature Mass Spectrometer

On the beam line BL2B in UVSOR a grazing incidence monochromator has been constructed which supplies photons in the energy region from 20 to 200 eV [M. Ono, H. Yoshida, H. Hattori and K. Mitsuke, *Nucl. Instrum. Methods Phys. Res., Sect. A* **467-468**, 577–580 (2001)]. This monochromator has bridged the energy gap between

the beam lines BL3B and BL4B, thus providing for an accelerating demand for the high-resolution and high-flux photon beam from the research fields of photoexcitation of inner-valence electrons, *L*-shell electrons in the third-row atom, and 4*d* electrons of the lanthanides.

Since 2001 we have tackled issues on photoabsorption and photofragmentation of fullerenes in the extreme UV. Geometrical structures and electronic properties of fullerenes have attracted widespread attention because of their novel structures, novel reactivity, and novel catalytic behaviors as typical nanometer-size materials. Moreover, it has been emphasized that the potential for the development of fullerenes to superconductors (T_c ~ 50 K) and strong ferromagnetic substances is extremely high. In spite of such important species spectroscopic information is very limited in the extreme UV region, which has been probably due to difficulties in obtaining enough amount of sample. The situation has been rapidly changed in these few years, since the techniques of syntheses, isolation, and purification have been advanced so rapidly that appreciable amount of fullerenes is obtainable from several distributors in Japan.

VI-H-1 Absolute Photoabsorption Cross Section of C_{60} in the Extreme Ultraviolet

MORI, Takanori; KOU, Junkei; HARUYAMA, Yusuke[1]; KUBOZONO, Yoshihiro[1]; MITSUKE, Koichiro
([1]Okayama Univ.)

[*J. Electron Spectrosc. Relat. Phenom.* **144-147**, 243–246 (2005)]

The absolute photoabsorption cross section curve of C_{60} has been determined by means of mass spectrometry with the photon source of monochromatized synchrotron radiation of $h\nu$ = 24.5–150 eV. Description has been made on a high-temperature source of gaseous fullerenes and an efficient time-of-flight mass spectrometer. The absolute cross section curve is shown in Figure 1. The obtained cross sections were 762, 241 and 195 Mb at $h\nu$ = 24.5, 90, and 110 eV, respectively with about 10% errors. The cross section curve was then normalized at $h\nu$ = 25 eV to the absolute photoabsorption cross section reported by Jaensch and Kamke,[1)] the most reliable data so far available in the valence excitation region of C_{60}. Accordingly, the present cross section data were altered to 407, 144 and 114 Mb at $h\nu$ = 25, 90, and 110 eV, respectively.

Reference

1) R. Jaensch and W. Kamke, *Mol. Materials* **13**, 143 (2000).

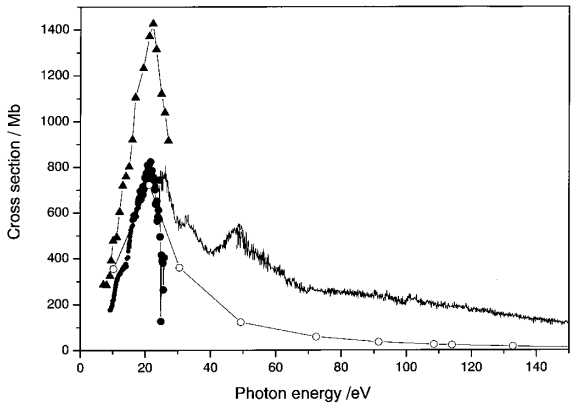

Figure 1. Absolute absorption cross section of C_{60} at $h\nu$ = 24.5–150 eV (solid line). The closed circles and triangles designate the previous data measured by Jaensch and Kamke and those compiled by Berkowitz, respectively. The open circles indicate the cross section of sixty carbon atoms.

VI-H-2 Photofragmentation of C_{60} in Valence Ionization

KOU, Junkei; MORI, Takanori; KUBOZONO, Yoshihiro[1]; MITSUKE, Koichiro
([1]Okayama Univ.)

[*J. Electron Spectrosc. Relat. Phenom.* **144-147**, 247–250 (2005)]

The yield curves for C_{60-2n}^+ (n = 1–3) produced by photoionization of C_{60} are measured in the $h\nu$ range of 25–150 eV. The appearance energies increase with increasing n, as evidenced from Figure 1. Evaluation is made on the upper limits of the internal energies of the primary C_{60}^+ above which $C_{60-2n+2}^+$ fragments ($n \geq 1$) cannot escape from further dissociating into $C_{60-2n}^+ + C_2$. These limits agree well with the theoretical internal energies of C_{60}^+ corresponding to the threshold for the formation of C_{60-2n}^+, on the assumption that the binding energies of $C_{60-2n+2}^+$ are equal to those proposed by Foltin *et al.*[1)]

Reference

1) M. Foltin, M. Lezius, P. Scheier and T. D. Märk, *J. Chem. Phys.* **98**, 9624 (1993).

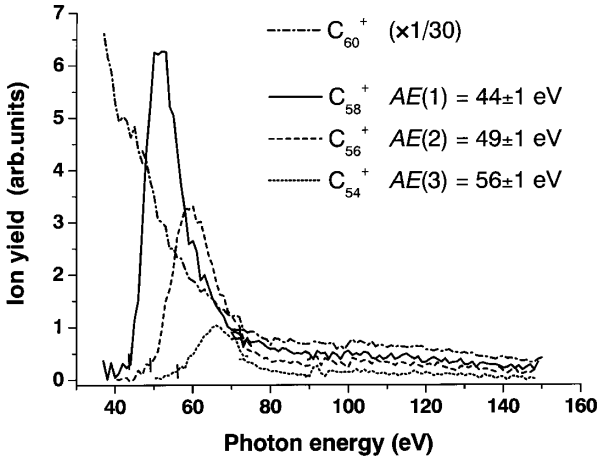

Figure 1. Ion yield curves of C_{60-2n}^+ (n = 1–3) and C_{60}^+ ions. Every tic mark indicates the appearance energy $AE(n)$ determined by, after subtracting an appropriate background, reading the photon energy at which the ion yield reaches 3% of the peak height of the curve.

VI-H-3 Photofragmentation of C_{60} in the Extreme Ultraviolet: Statistical Analysis on the Appearance Energies of C_{60-2n}^{z+} ($n \geq 1$, $z = 1–3$)

KOU, Junkei; MORI, Takanori; KUBOZONO, Yoshihiro[1]; MITSUKE, Koichiro
([1]Okayama Univ.)

[*Phys. Chem. Chem. Phys.* **7**, 119–123 (2005)]

The ion yield curves for C_{60-2n}^{z+} (n = 1–5, z = 1–3) produced by photoionizaiotion of C_{60} are measured in the photon energy ($h\nu$) range of 25–150 eV (see Figure 1). The appearance $h\nu$ values are higher by 30–33 eV than the thermochemical thresholds for dissociative ionization of C_{60} leading to C_{60-2n}^{z+}. Evaluation is made on the upper limits of the internal energies of the primary C_{60}^{z+} above which $C_{60-2n+2}^{z+}$ fragments ($n \geq 1$) cannot escape from further dissociating into C_{60-2n}^{z+} + C_2. These upper limits agree well with the theoretical internal energies of C_{60}^{z+} corresponding to the threshold for the formation of C_{60-2n}^{z+} (see Figure 2). The photofragmentation of C_{60}^{z+} is considered to be governed by the mechanism of internal conversion of the electronically excited states of C_{60}^{z+}, statistical redistribution of the excess energy among a number of vibrational modes, and sequential ejection of the C_2 units.

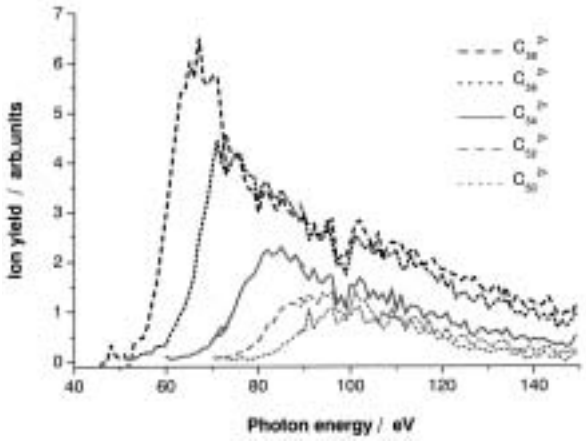

Figure 1. Ion yield curves of C_{60-2n}^{2+} ions (n = 1–5) obtained from time-of-flight mass spectra.

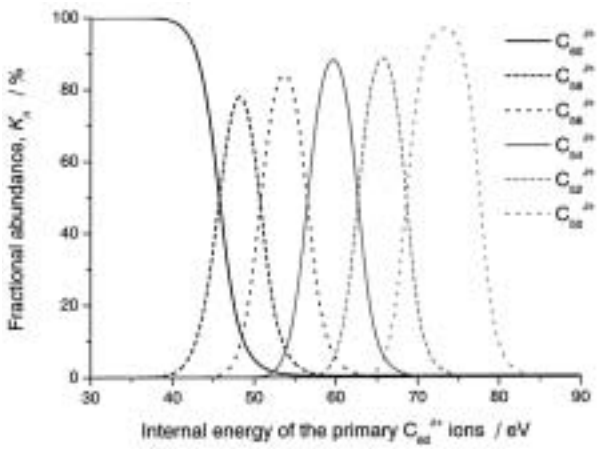

Figure 2. Fractional abundance curves of C_{60}^{z+} and C_{60-2n}^{z+} ions (n = 1–5) at 25 μs after photoionization of C_{60} obtained by using the RRKM theory to calculate the rate constant for reaction $C_{60-2n+2}^{z+}$ ($n \geq 1$) → C_{60-2n}^{z+} + C_2.

VI-H-4 Fragmentation Mechanism of Highly Excited C_{70} Cations in the Extreme Ultraviolet

MITSUKE, Koichiro; KATAYANAGI, Hideki; KOU, Junkei; MORI, Takanori; KUBOZONO, Yoshihiro[1]
([1]Okayama Univ.)

[*Am. Inst. Phys. Conf. Proc.* in press]

The ion yield curves for C_{70-2n}^{z+} (n = 1–8, z = 2 and 3) produced by photoionization of C_{70} were measured in the photon energy ($h\nu$) range of 25–150 eV. The appearance $h\nu$ values were higher by *ca.* 34 eV than the thermochemical thresholds for dissociative ionization of C_{70} leading to C_{70-2n}^{z+}. Evaluation was made on the upper limits of the internal energies of the primary C_{70}^{z+} above which $C_{70-2n+2}^{z+}$ fragments cannot escape from further dissociating into C_{70-2n}^{z+} + C_2. These critical internal energies agreed well with appearance internal energies of C_{70}^{z+} theoretically obtained corresponding to the threshold for the formation of C_{70-2n}^{z+} (see Figure 1). The photofragmentation of the parent C_{70}^{z+} ions is considered to be governed by the mechanism of internal conversion of their electronically excited states, statistical redistribution of the excess energy among a number of vibrational modes, and sequential ejection of the C_2 units.

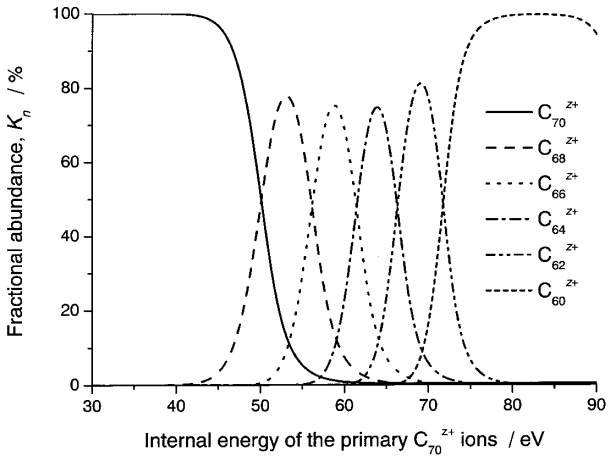

Figure 1. Fractional abundance curves of C_{70}^{z+} and C_{70-2n}^{z+} ions at 25 μs after photoionization of C_{70} obtained by using the RRKM model to calculate the rate constants for reaction $C_{70-2n+2}^{z+}$ ($n \geq 1$) → C_{70-2n}^{z+} + C_2.

VI-H-5 $4d \rightarrow 4f$ Dipole Resonance of the Metal Atom Encapsulated in a Fullerene Cage: Ce@C_{82}

MITSUKE, Koichiro; MORI, Takanori; KOU, Junkei; HARUYAMA, Yusuke[1]; KUBOZONO, Yoshihiro[1]
([1]Okayama Univ.)

[*J. Chem. Phys.* **122**, 064304 (5 pages) (2005)]

The yield curves for photoions from $Ce@C_{82}$ are measured by using synchrotron radiation in the photon energy range from 90 to 160 eV. Parent $Ce@C_{82}^{z+}$ and fragment ions C_{60}^{z+} and C_{70}^{z+} are observed in a mass spectrum (z = 1 and 2) as shown in Figure 1. The yield curves for doubly-charged ionic species exhibit broad resonance in the photon energy region of from 120 to 140 eV which is ascribed to the $4d \rightarrow 4f$ giant dipole resonance of the encapsulated Ce atom. The total photoabsorption cross section of $Ce@C_{82}$ was determined from partial photoionization cross sections for formation of the parent and fragment ions to be $5.3^{+1.8}_{-1.1}$ and $19.6^{+6.5}_{-3.9}$ Mb at photon energies of 110 and 130 eV, respectively.

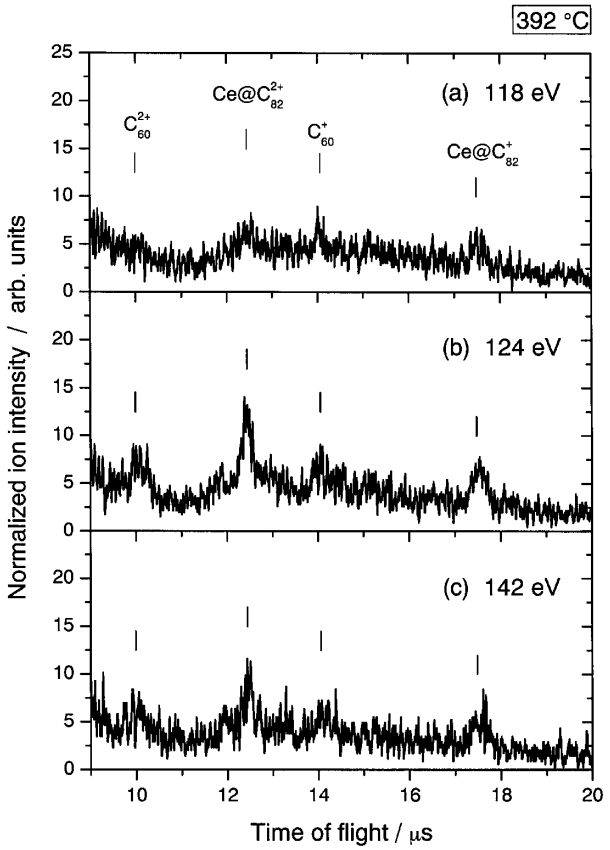

Figure 1. Time-of-flight mass spectra of the $Ce@C_{82}^{z+}$ (z = 1 and 2) produced by photoionization of $Ce@C_{82}$ at $h\nu$ = 118, 124, and 142 eV. The average temperature of the sample holder was set to 392 °C. Most of C_{60}^{z+} ions arose from photoionization of C_{60} neutrals which were desorbed from the surface of mass spectrometer.

VI-H-6 Photoion Yield Curves of Dy@C_{82} in the Vacuum UV Region

MITSUKE, Koichiro; MORI, Takanori; KOU, Junkei; HARUYAMA, Yusuke[1]; TAKABAYASHI, Yasuhiro[1]; KUBOZONO, Yoshihiro[1]
([1]Okayama Univ.)

[*Int. J. Mass Spectrom.* **243**, 121–125 (2005)]

The photoion yield curves for $Dy@C_{82}^{z+}$ (z = 1 and 2) from $Dy@C_{82}$ are measured by using synchrotron radiation in the photon energy range from 24.5 to 39.5 eV. Correction has been made to compensate the effect of transient change of the density of $Dy@C_{82}$ in the interaction region, with the help of the yield curve of C_{60}^{z+} produced from C_{60} remaining as a trace impurity in the sample. The yield of $Dy@C_{82}^{+}$ in Figure 1 exhibits a gradually descending curve with a flat region at 30–33 eV, similarly to the yield curve of C_{60}^{+} from C_{60}. The total photoabsotpion cross section of $Dy@C_{82}$ was evaluated to be $(1.2\pm0.4) \times 10^2$ Mb at the photon energy of 39.5 eV.

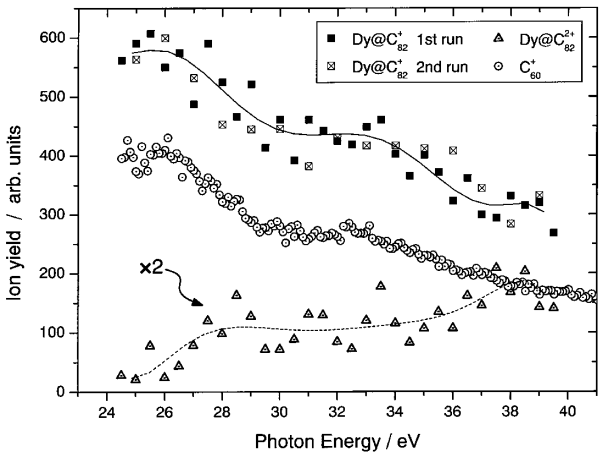

Figure 1. Yield curves of $Dy@C_{82}^{+}$ (solid square) and $Dy@C_{82}^{2+}$ (open triangle) produced from $Dy@C_{82}$ in the photon energy range of from 24.5–39.5 eV. The spectra are taken at photon energy intervals of 0.5 eV. The solid and dashed curves represent the results of the least-squares fitting to the data points of $Dy@C_{82}^{+}$ and $Dy@C_{82}^{2+}$, respectively, using seventh order polynomial functions. The open circle symbols denote the yield curve of C_{60}^{+} from C_{60} measured by using the neat C_{60} sample.

VI-H-7 4*d*–4*f* Dipole Resonance of the Pr Atom in an Endohedral Metallofullerene, Pr@C_{82}

KATAYANAGI, Hideki; KAFLE, Bhim Prasad[1]; KOU, Junkei; MORI, Takanori; MITSUKE, Koichiro; TAKABAYASHI, Yasuhiro[2]; KUWAHARA, Eiji[2]; KUBOZONO, Yoshihiro[2]
([1]SOKENDAI; [2]Okayama Univ.)

Following our preceding paper on the photoion yield spectra of the endohedral metallofullerene, $Ce@C_{82}$,[1)] photoion yield spectra of $Pr@C_{82}$ were measured in the photon energy range 100–150 eV with the help of time-of-flight mass spectrometry. Parent ions, $Pr@C_{82}^{+}$, $Pr@C_{82}^{2+}$ and $Pr@C_{82}^{3+}$ were observed in the mass spectra. Photoion yield spectra of $Pr@C_{82}^{+}$ and $Pr@C_{82}^{2+}$ were obtained from the mass spectra and are shown in Figure 1. The photoion yield spectra of $Pr@C_{82}^{2+}$ showed a broad peak at 120–140 eV. The broad peak was assigned to the $4d \rightarrow 4f$ giant dipole resonance of the encapsulated Pr atoms. Absolute photoabsorption cross sections of $Pr@C_{82}$ were evaluated from the photoion yield spectra and found to be 23.6±6.7 at 110 eV (off-resonance) and 35.0±6.3 Mb at 130 eV (on-resonance).

The enhancement of photoabsorption due to the giant resonance was comparable to that in Ce@C_{82}. The shapes of the peaks in the Pr@C_{82} spectra, which originated from interference effects induced by the fullerene cage, were, however, different from those in the Ce@C_{82} spectra. This could be accounted for by that the interference effects depend on the interior metal atoms.

Reference

1) K. Mitsuke, T. Mori, J. Kou, Y. Haruyama and Y. Kubozono, *J. Chem. Phys.* **122**, 064304 (2005).

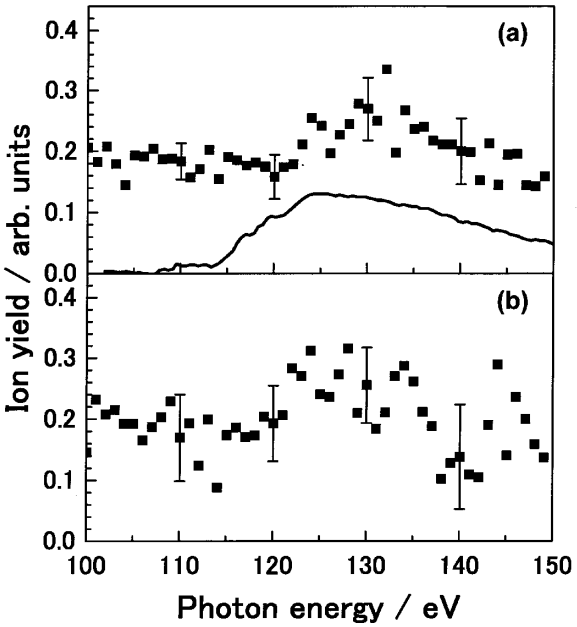

Figure 1. Ion yield curves of (a) Pr@C_{82}^{2+} and (b) Pr@C_{82}^{+}. Error bars correspond to 1σ of five experimental runs. Solid curve in (1) are the absorption spectra of Pr atoms. For each data, the vertical scaling is arbitrary.

VI-I Kinetic Energy Analysis of the Fragment ions Produced from Fullerenes

When fullerenes gain enough amount of energy through photoionization processes, primarily formed ions are known to undergo decomposition into fragment ions with even numbered carbon atoms via sequential loss of C_2 units. We have measured the yield curves for C_{60-2n}^{z+} from C_{60} as a function of the internal energy of the parent C_{60}^{z+} ions to study the mechanisms and kinetics of the sequential unimolecular reactions. These experimental yield curves have been compared with the theoretical fractional abundance curves which have been derived by employing the RRKM theory to every process of the sequential reactions: $C_{60-2n+2}^{z+}$ ($n \geq 1$) → C_{60-2n}^{z+} + C_2. To a first approximation the critical activation energies of the reactants $C_{60-2n+2}^{z+}$ were assumed to be equal to their binding energies for the above reactions. Indeed the experimental and theoretical curves provide almost the same appearance energies for the formation of C_{60-2n}^{z+} ($n \geq 1$). More reliable calculations of the rate constants of the individual reactions are needed before closer comparison between the two curves will be made. For such calculations we must know precise values of the activation energies for the reactions, together with the vibrational spectra of the transition states. This induced us to develop a new ion spectrometer for the fragment ions produced from C_{60}^{z+} and C_{70}^{z+}. We wish that the magnitude of the potential barriers of the reactions can be estimated from the average kinetic energy release measured by this spectrometer.

VI–I–1 Development of the Photofragment Imaging Apparatus to Measure Scattering Distributions of the C_{60-2n}^{z+} and C_{70-2n}^{z+} Fragments Produced by Dissociative Photoionization of C_{60} and C_{70}

KAFLE, Bhim Prasad[1]; KATAYANAGI, Hideki; MITSUKE, Koichiro
([1]SOKENDAI)

In dissociative photoionization of solitary fullerenes (C_{60}, C_{70}), we have measured the photofragment (C_{60-2n}^{z+}, C_{70-2n}^{z+}) yield curves in the photon energy range of 45–150 eV.[1)] From the results we concluded that the excess energy is statistically distributed among the internal degrees of freedom of the parent ions (C_{60}^{z+}, C_{70}^{z+}) and C_2 units are ejected sequentially. Moreover, the results imply that the dissociation has no barrier and that no resonant state participates in the dissociation. To clarify these implications, we designed the photofragment imaging apparatus on the basis of the time-of-flight mass spectrometer that we had constructed. From the photofragment images, we can extract the kinetic energy and angular distributions of the photofragments. These distributions reveal clearly whether there exist a barrier and/or resonance.

We adopted the Eppink-Parker type velocity focusing electrodes[2] to achieve the energy resolution on the images to resolve less than 0.1 eV increase by the photofragmentation. To select a bunch of fragments having a desired mass from neighboring bunches, for example, selecting C_{66}^+ from the consecutive masses such as C_{68}^+, C_{66}^+ and C_{64}^+, we designed a "mass gate" which consists of a potential switch and retarding electrodes. In order to optimize the dimensions of the setup, we performed ion trajectory simulations utilizing SIMION 7.0 software. The most suitable dimensions were obtained already and are schematically illustrated in Figure 1.

The operation principle of this setup is as follows. As long as the tube of the potential switch is kept grounded, all fragments are reflected back by the retarding electrode and do not hit an imaging detector. When an entire bunch of fragments having a desired mass enters inside the tube, the pulsed voltage is applied to the tube. The potential felt by the bunch are suddenly elevated and the bunch passes through the retarding electrode and thus hits the imaging detector.

Parts of this setup are being fabricated at the machine shop in IMS. The parts will be installed in the end-station at the beam line 2B in UVSOR. We are planning to examine the performance of the setup using SF_6 as a standard sample.

References

1) J. Kou, T. Mori, Y. Kubozono and K. Mitsuke, *Phys. Chem. Chem. Phys.* **7**, 119 (2005).
2) A. T. J. B. Eppink and D. H. Parker, *Rev. Sci. Instrum.* **68**, 3477 (1997).

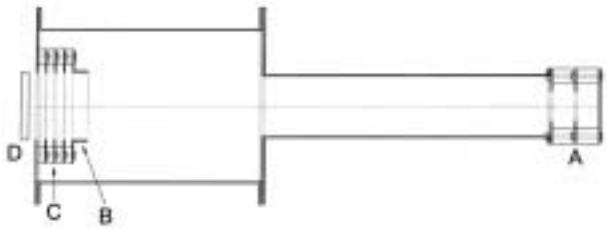

Figure 1. Schematic illustration of the photofragment imaging apparatus. A, repeller and extractor; B, potential switch; C, retarding electrodes; D, imaging detector.